minerals

MDPI

Article

Metal Sources of World-Class Polymetallic W–Sn Skarns in the Nanling Range, South China: Granites versus Sedimentary Rocks?

Weicheng Jiang [1], Huan Li [2,*], Noreen J. Evans [3], Jinghua Wu [1] and Jingya Cao [4]

1 Department of Resources Science and Engineering, Faculty of Earth Resources, China University of Geosciences, Wuhan 430074, China; wcjiang@cug.edu.cn (W.J.); jhwu@cug.edu.cn (J.W.)
2 Key Laboratory of Metallogenic Prediction of Nonferrous Metals and Geological Environment Monitoring, Ministry of Education, School of Geosciences and Info-Physics, Central South University, Changsha 410083, China
3 School of Earth and Planetary Science, John de Laeter Centre, TIGeR, Curtin University, Bentley, WA 6845, Australia; noreen.evans@curtin.edu.au
4 CAS Key Laboratory of Crust–Mantle Materials and Environments, School of Earth and Space Sciences, University of Science and Technology of China, Hefei 230026, China; jingyacao@126.com
* Correspondence: lihuan@csu.edu.cn

Received: 25 May 2018; Accepted: 20 June 2018; Published: 24 June 2018

Abstract: Widespread, large-scale polymetallic W–Sn mineralization occurs throughout the Nanling Range (South China) dated 160–150 Ma, and related to widely developed coeval granitic magmatism. Although intense research has been carried out on these deposits, the relative contribution of ore-forming elements either from granites or from surrounding strata is still debated. In addition, the factors controlling the primary metallogenic element in any given skarn deposit (e.g., W-dominated or Sn-dominated) are still unclear. Here, we select three of the most significant skarn-deposits (i.e., Huangshaping W–Mo–Sn, Shizhuyuan W–Sn–Mo–Bi and Xianghualing Sn), and compare their whole-rock geochemistry with the composition of associated granites and strata. The contents of Si, Al and most trace elements in skarns are controlled by the parent granite, whereas their Fe, Ca, Mg, Mn, Ti, Sr and REE patterns are strongly influenced by the wall rock. Samples from the Huangshaping skarn vary substantially in elemental composition, probably indicating their varied protoliths. Strata at the Shizhuyuan deposit exerted a strong control during metasomatism, whereas this occurred to a lesser degree at Huangshaping and Xianghualing. This correlates with increasing magma differentiation and increasing reduction state of granitic magmas, which along with the degree of stratigraphic fluid circulation, exert the primary control on dominant metallogenic species. We propose that wall rock sediments played an important role in the formation of W–Sn polymetallic mineralization in South China.

Keywords: W–Sn skarn; whole-rock geochemistry; Huangshaping; Shizhuyuan; Xianghualing

1. Introduction

Most skarn deposits are formed by the interaction between shallow magmatic systems and carbonate rocks [1–4]. Since the 1990s, the trace element (and particularly rare earth element; REE) characteristics of skarn-associated plutons and their constituent minerals have been the focus of much research given that these signatures reveal much about deposit genesis [5–10]. Major and accessory mineral phases in skarns (such as garnet and scheelite) inherit their REE patterns from magmatic fluids and they control the REE signatures of the host skarn [11]. However, Giuliani et al. [12] propose that strong REE variations in skarns, characterized by a pronounced negative Eu anomaly and low

La/Yb ratios, result from the interaction between scheelite and the surrounding metamorphic rocks. In addition, REE signatures are affected by the distance of the skarn from the related intrusive body, with REE concentrating in skarns during prograde alteration and migrating outward of the skarns during retrograde alteration [13]. Furthermore, Alirezaei et al. [8] note that skarns vary in texture from massive to banded and that textural contrast is reflected in their whole rock composition: Fe, Si and S are significantly enriched, and Na, large ion lithophile elements (LILE) and light REE (LREE) are strongly depleted in the massive skarns while Na, K, Si, and S are slightly enriched in the banded skarns. Siesgesmund et al. [14] recently note that LILE (K, Rb, Ba, Sr) and REE are moderately depleted and high field strength elements (HFSE) are slightly enriched in Cu–Au skarns, relative to the intrusive rocks. Correlations between major and trace elements in skarns are weak or absent, but skarn REE patterns can be used as a prospectivity indicator in a metallogenic system [15]. However, it is still confused whether the chemical composition of ore-related skarns is correlated with the size of relevant deposit and the primary metallogenic elements enriched in skarns. Determining whether the composition of skarns can be used to indicate the metal source of skarn-type deposits requires further research.

The Nanling Range (Figure 1a), located in the central part of South China, represents the largest W–Sn ore province in the world. More than 30 Mesozoic granite-related skarn-type polymetallic deposits are distributed across this region, represented by the large Shizhuyuan, Xianghualing, Huangshaping, Xintianling, Furong, Baoshan and Yaogangxian deposits (Figure 1b) [16–20]. These deposits mainly comprise nonferrous, rare and base metal elements, such as W, Sn, Mo, Bi, Li, Be, Nb, Ta, Cu, Au, Ag, Pb, Zn, U and REE [20–27]. Given the economic significance of these deposits, a great deal of research has focused on skarn minerals, including the study of mineralogy, geochemistry, geochronology, formation temperature and pressure, and fluid and ore associations [28–37]. It is traditionally believed that extensive Mesozoic magmatism is one of the primary factors responsible for the formation of coeval polymetallic deposits [9,16,34,38–40], and that ore-forming elements are mainly derived from parent granitic plutons with minor input from the surrounding strata [11,28,33,34,41–43]. However, the strata contribution to the ore element budget may previously have been underestimated. Chen et al. [44] propose that ore-forming metals such as W and Sn are extracted from country rocks by high temperature circulating water and metamorphic fluids released from deep crustal rocks. In addition, systematic and comprehensive studies comparing the behavior of major and trace elements in different types of skarn-related bodies (granites and host strata) at the time of ore formation are lacking. Understanding the behavior of elements during metasomatism, in both the pluton and wallrock, would elucidate metal sources and enhance current exploration models.

In this paper, the whole rock major and trace element geochemistry of three typical Nanling Range skarn-type deposits with different primary metal enhancements are studied (Huangshaping W–Mo–Sn, Shizhuyuan W–Sn–Mo–Bi and Xianghualing Sn deposits). By comparing the chemical composition of these skarns, the related granites and the sedimentary host rocks, this study aims to elucidate the controls on the nature of the metals and deposit size and providing new insights into the genesis of large-scale polymetallic skarn-type deposits in the Nanling Range.

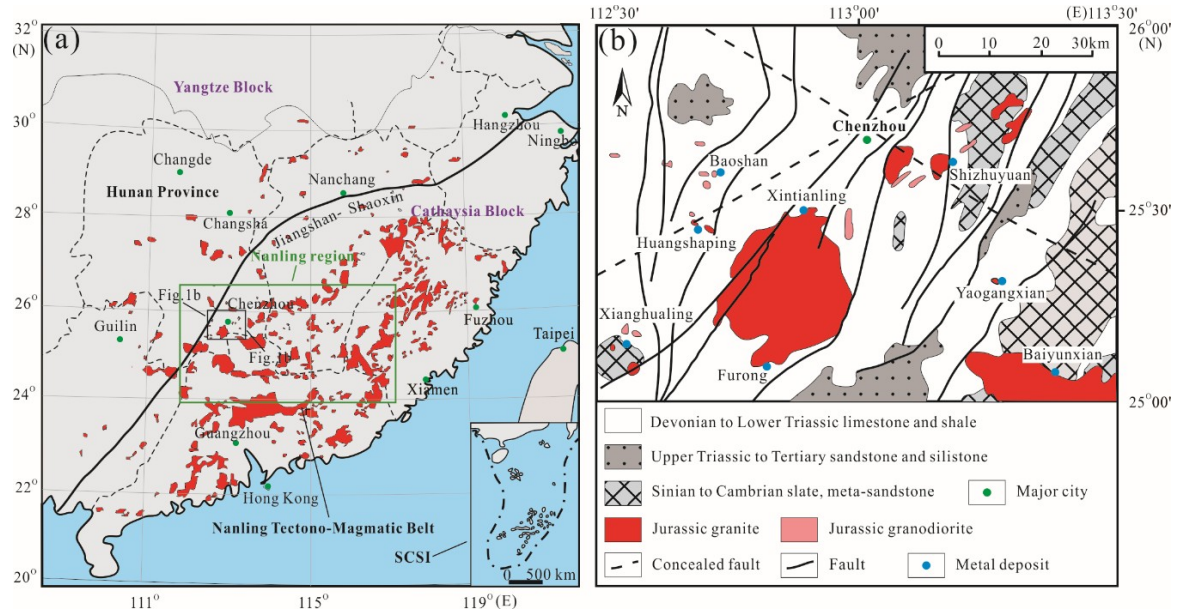

Figure 1. Regional geological map. (**a**) Simplified geological sketch map showing the distribution of Jurassic granitoids in South China (after [24]); (**b**) Geological sketch map of W–Sn polymetallic deposits in the central Nanling Range, southern Hunan (modified from [22]).

2. Geological Setting

2.1. Regional Geology

The South China Block comprises by two major terranes: the Yangtze block in the northwest and the Cathaysia block in the southeast (Figure 1a) [45], amalgamated along the Jiangnan Orogen during the Neoproterozoic [46–51].

The Nanling Range is in the center of the South China Block (Figure 1a). Geographically, it contains most of the bordering areas of the Hunan, Jiangxi, Fujian, Guangdong and Guangxi provinces. Mesozoic (especially Jurassic) granitoids, characterized by calc-alkaline A-type granites, are distributed throughout the area [39,52,53]. The sedimentary rocks within the Nanling Range can be divided into three groups: (1) Late Proterozoic basement composed of thick-bedded (metamorphic) detrital sedimentary rocks that are overlain by (2) Devonian–Triassic carbonate rocks and marls intercalated with clastic rock and then by (3) Jurassic–Cretaceous detrital and volcanic rocks deposited in rifted basins [17,54]. The Nanling Range has been affected by multiple episodes of tectonic activity since the Phanerozoic [55,56]. The structural framework of the Nanling Range was primarily controlled by both the Tethyan tectonic domain and the Indosinian orogenesis pre-Jurassic, but later overprinted by Pacific plate tectonism and intracontinental deep structures [57,58]. A three-stage Mesozoic tectonic evolution is proposed by Shu et al. [59] based on sedimentary basin analysis: (1) Late Triassic–Early Jurassic post-orogenic stage; (2) Middle Jurassic tectonic rifting stage and (3) Cretaceous intracontinental extension and faulted-depression stage.

2.2. Deposit Geology

2.2.1. The Huangshaping W–Mo–Sn Polymetallic Skarn Deposit

The Huangshaping deposit, located southwest of Chenzhou City (Figure 1b), is one of the most important W–Mo–Sn polymetallic skarn deposits in the Hunan province. The outcropping strata in this area are mainly clastic and carbonate rocks, consisting of the Upper Devonian Shetianqiao and Xikuangshan Formations and Lower Carboniferous Ceshui, Menggong'ao, Shidengzi and Zimenqiao Formations, respectively (Figure 2a). Among them, the Shidengzi limestones are the richest host rocks,

followed by the Ceshui sandstones and shales and the Zimenqiao dolomite. There are several episodes of magmatic activity in the Huangshaping area between 180 and 150 Ma. Among them, the granite porphyry, the latest and most evolved intrusive phase, is regarded as the most important metal source and host rock of the skarns [60–62].

At Huangshaping, the dominant mineralization type hosted by the granite porphyry is W–Mo–Sn skarn-type ore (WO_3 = 0.15 Mt and its grade = 0.2%; Mo = 0.043 Mt and its grade = 0.06%) [24,61,62]. The ore is mainly located between granite porphyry and carbonate rocks and along faults (Figures 3a and 4a,b). The skarn-forming metasomatism can be further subdivided into two stages in terms of the mineral assemblages: the early stage prograde skarn contains garnet, diopside and fluorite while the late stage retrograde skarn is dominated by tremolite and magnetite [35,63].

2.2.2. The Shizhuyuan W–Sn–Mo–Bi Polymetallic Skarn Deposit

The Shizhuyuan deposit is located to the southeast of Chenzhou City (Figure 1b), and is often referred to as the "nonferrous metal museum" due to the variety of mineralizing elements. The Middle-Upper Devonian Qiziqiao and Shetianqiao limestones and dolomitic limestones are the most favorable hosts of metal mineralization at Shizhuyuan (Figure 2b). The formation of the large Shizhuyuan deposit is related to the emplacement of the Qianlishan granite complex, with significant metal reserves of W (0.71 Mt with grade of 0.31%), Sn (0.48 Mt with grade of 0.14%), Mo (0.12 Mt with grade of 0.054%) and Bi (0.27 Mt with grade of 0.11%) (unpublished data from [64]). The Qianlishan complex is characterized by a small outcrop area (9.7 km^2) and multistage magmatic-hydrothermal activity from 158 to 151 Ma [44,65–68]. Three main episodes of magmatism can be distinguished in chronological order: (1) porphyritic biotite granite; (2) equigranular biotite granite and (3) granite porphyry [39,67–69]. Among them, the equigranular biotite granite is believed to have the closest relationship to the skarn-forming metasomatism [28].

The skarn mineralization at Shizhuyuan can be divided into massive-type and vein-type based on their textures, and vesuvianite-wollastonite skarn (ore-free) and garnet-diopside skarn (ore-bearing) by mineral assemblages, respectively [25,70,71]. Skarn mineralization can also be divided into two stages: (1) early stage massive W–Sn–Mo–Bi (Figures 3b and 4c,d); and (2) late stage vein-type W–Sn–Mo–Bi–Be–Pb–Zn–Ag [70].

2.2.3. The Xianghualing Sn Polymetallic Skarn Deposit

The Xianghualing deposit is located about 60 km from Chenzhou City. The exposed strata in the Xianghualing area comprise Cambrian to Quarternary sequences, with no Ordovician and Silurian strata present. The main ore-hosting layers are Cambrian slates and meta-sandstones, as well as Devonian carbonate rocks of the Qiziqiao and Shetianqiao Formations (Figure 2c). The Sn mineralization of the Xianghualing deposit is hosted by the Laiziling pluton, with albite granite as its major rock type [72]. Based on geochronological studies, the crystallization age of the Laiziling granite is about 155–150 Ma [23,33,39,73,74].

Mainly mineralized by Sn, the skarn orebodies in the Xianghualing deposit are mainly stratiform, pipe or vein-like, distributed in the contact zone between albite granite and sedimentary rocks along faults (Figure 3c), or within the formation unconformity. The total metal reserve of Sn is estimated at 0.76 Mt (unpublished mining data from the local geological survey) and skarn-type cassiterite-arsenopyrite-pyrrhotite ore is the most economic mineralization (Figure 4e,f).

2.3. Petrology and Mineralogy of Skarns

2.3.1. The Huangshaping Skarn

The Huangshaping skarn is dark green with bronze or brown irregular mineral lumps on the surface, blastic texture and massive structure, dominated by W–Mo–Sn mineralization (Figure 5a). The skarn can be divided into garnet skarn and pyroxene skarn, which formed in the proximal and distal portions of the granite porphyry, respectively. The garnet is mainly grossularite (Figure 5b) and andradite, whereas

the pyroxene is dominated by hedenbergite. The garnet skarn can be classified into two sub-types: (1) granite-related type with rufous color, inhomogeneous granularity and dense massive structure; and (2) exoskarn with coarse-grained texture and dark brown or green color. The latter is associated with abundant hydrous skarn minerals (e.g., actinolite, vesuvianite and hornblende) [35].

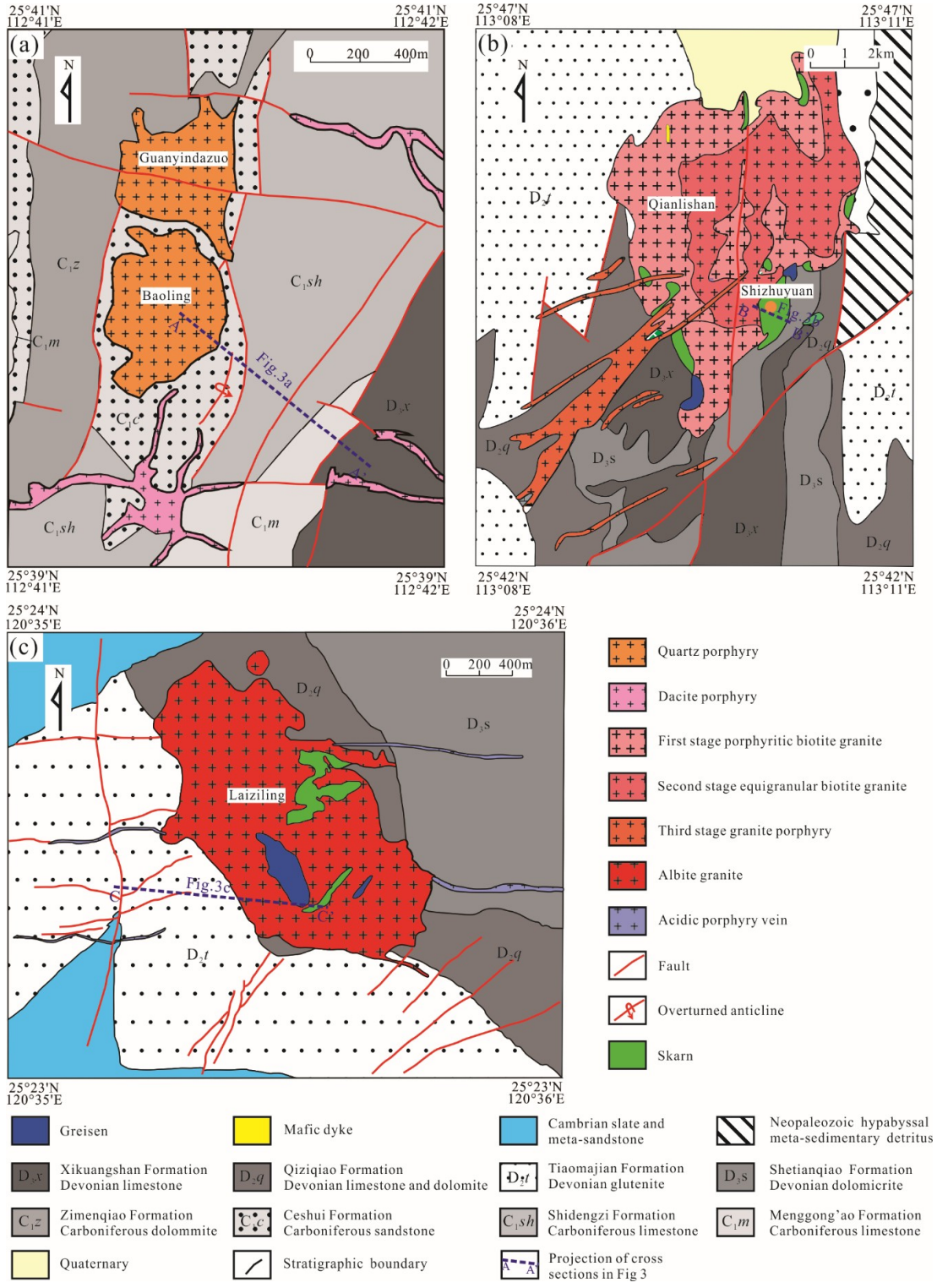

Figure 2. Geological maps of (**a**) the Huangshaping deposit (modified from [24]); (**b**) the Shizhuyuan deposit (modified from [68]); and (**c**) the Xianghualing deposit.

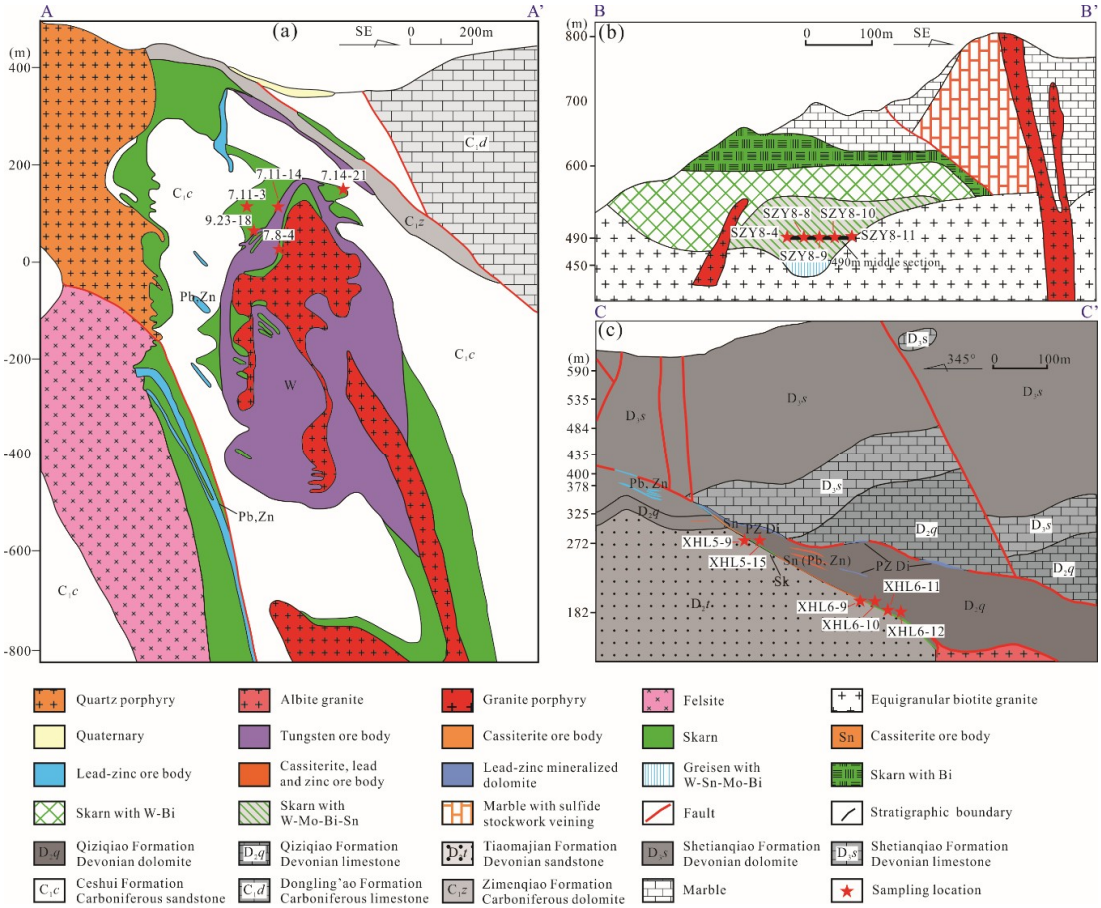

Figure 3. Cross-sections of (**a**) the Huangshaping deposit, (**b**) the Shizhuyuan deposit (modified from [11]); and (**c**) the Xianghualing deposit, respectively.

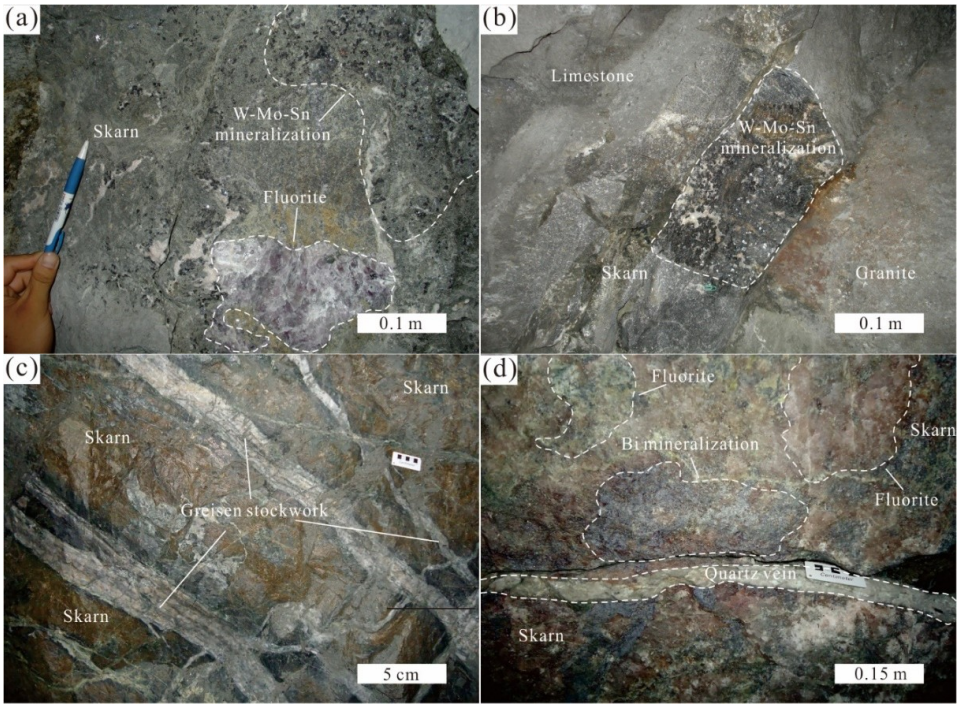

Figure 4. *Cont*.

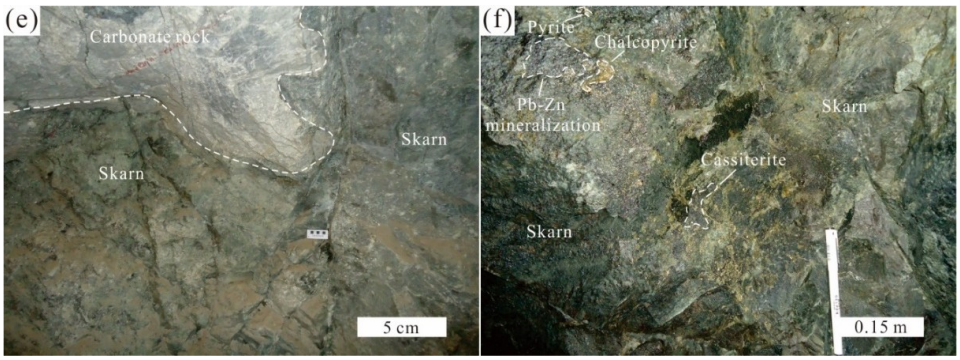

Figure 4. Field occurrences of ore-related skarns. The Huangshaping deposit: (**a**) fluorite and W–Mo–Sn mineralization developed in massive skarn; (**b**) W–Mo–Sn mineralization located at the contact zone between limestone and granite. The Shizhuyuan deposit: (**c**) greisen stockwork interweave within massive skarn; (**d**) fluoritization, Bi mineralization and quartz veins in massive skarn. The Xianghualing deposit: (**e**) contacting relationship between carbonate rock and skarn; (**f**) massive skarn mineralized by galena, sphalerite, pyrite, chalcopyrite and cassiterite.

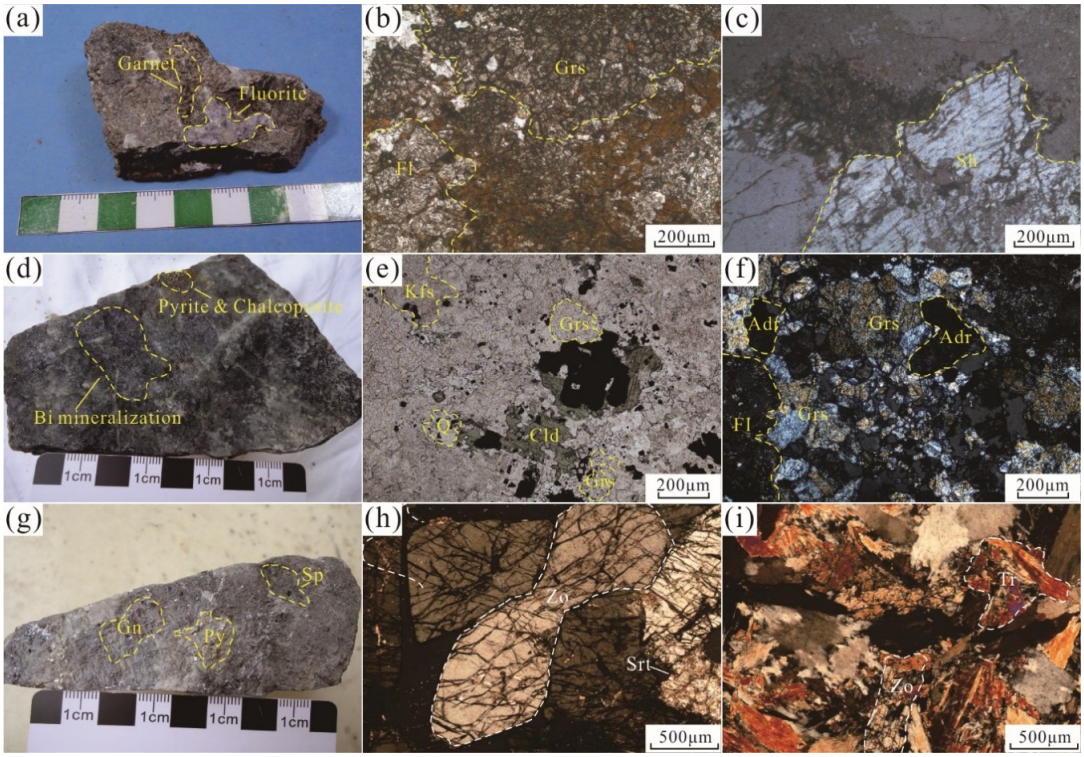

Figure 5. Photos of hand specimen and thin sections of skarn samples. The Huangshaping deposit: (**a**) garnet-fluorite skarn, (**b**) grossularite and fluorite in garnet skarn, (**c**) scheelite mineralization in garnet skarn; The Shizhuyuan deposit: (**d**) Bi-mineralized skarn, (**e**) grossularite, chloritoid, quartz and feldspar in ore-bearing garnet skarn, (**f**) grossularite, andradite and fluorite in ore-bearing garnet skarn; The Xianghualing deposit: (**g**) Sn-mineralized skarn ore, (**h**) zoisite and sericite in skarn, (**i**) zoisite and tremolite in skarn. Adr: andradite; Cld: Chloritoid; Fl: fluorite; Gn: galena; Grs: grossularite; Kfs: K-feldspar; Sh: scheelite; Sp: sphalerite; Srt: sericite; Py: pyrite; Q: quartz; Tr: tremolite; Zo: zoisite.

Besides garnet and pyroxene, other minerals in the Huangshaping skarn include chlorite, calcite, fluorite, feldspar and quartz. In addition, metal-bearing minerals include scheelite (Figure 5c), molybdenite, cassiterite, arsenopyrite, pyrite, chalcopyrite, pyrrhotite, magnetite, galena and sphalerite.

2.3.2. The Shizhuyuan Skarn

The Shizhuyuan skarn is brownish-red to gray-green in color, with granoblastic, granular and crystalloblastic textures and massive, comb and banded structures (Figure 5d).

The dominant minerals of the Shizhuyuan skarns are garnet, followed by pyroxene, wollastonite and vesuvianite. Compositionally, pyroxene mainly comprises hedenbergite and diopside, while the garnet belongs to the grossularite-andradite series. According to the mineral paragenesis, garnets from the Shizhuyuan skarn can be classified into early and late stages. The early garnet is characterized by euhedral granular texture whereas the late-stage garnet is a veinlet-type with bright red color and larger single crystal [75].

Additional skarn minerals are chlorite, epidote, actinolite and hornblende as well as fluorite. Most metallic minerals are hosted by massive garnet-pyroxene skarns (Figure 5e,f), including scheelite, wolframite, molybdenite, cassiterite, bismuthinite, pyrite, pyrrhotite, chalcopyrite, magnetite, galena and sphalerite.

2.3.3. The Xianghualing Skarn

The gray to dark green Xianghualing skarn has a granular to crystalloblastic texture and a massive structure (Figure 5g). The skarn has a variety of mineral assemblages: (1) skarn developed near the metasomatic contact zone is dominanted by diopside, wollastonite, vesuvianite and zoisite (Figure 5h) with minor garnet; (2) skarn controlled by fractures or structures is mainly composed of diopside, actinolite, tremolite (Figure 5i) and vesuvianite; and (3) skarn located at the unconformity between Devonian and Cambrian strata mainly consists of actinolite, associated with silicification [33]. Ore minerals in the skarn are dominated by cassiterite, followed by pyrite, pyrrhotite, arsenopyrite, stannite, galena, sphalerite, magnetite and chalcopyrite.

3. Sampling and Analytical Methods

All skarn samples were collected from underground adits or drill cores (Figure 3), and only the freshest material was analyzed (supplementary materials). From the Huangshaping skarn, samples 7.11–3 and 7.11–14 were collected at Level 96 m, from the west side of the granite porphyry pluton; sample 7.8–4 was collected from Level 20 m; sample 7.14–21 was collected from Level 136 m; and sample 9.23–18 was collected at Level 56 m. All the Shizhuyuan skarn samples (SZY8-4, SZY8-8, SZY8-9, SZY8-10 and SZY8-11) were collected at Level 490 m, close to the equigranular biotite granite. From the Xianghualing skarn, samples XHL5-9, XHL5-15, XHL6-9 and XHL6-10 were collected at Level 272 m near the fault F1, whereas samples XHL6-11 and XHL6-12 were collected at Level 182 m, closely related to the albite granite.

After sampling, each sample was cut for thin sections and the remainder was crushed to >200 mesh size using an iron pestle and mortar. From the Huangshaping skarn, major element analysis was conducted at Kyushu University (Fukuoka, Japan), using X-ray fluorescence spectrometry (XRF, Rigaku RIX 3100, Tokyo, Japan), and the trace elements were determined by inductively coupled plasma mass spectrometry (ICP-MS, Perkin Elmer Elan 9000, Perkin, Waltham, MA, USA) at the ALS Laboratory in Vancouver, Canada. The XRF (Panalytical, Almelo, The Netherlands) and ICP-MS (Perkin Elmer Elan 9000, Perkin, Waltham, MA, USA) analysis of the whole-rock compositions for the Xianghualing and Shizhuyuan skarns was carried out at the ALS Laboratory in Guangzhou, China. For analysis of major elements, samples were decomposed by lithium borate fusion, and the major elements were analyzed by XRF with a determination of loss-on-ignition at 1000 °C. The "total" is a combination of all data. The analytical process for trace element analysis is as follows: A prepared sample was added to a lithium metaborate/lithium tetraborate flux, mixed well and fused at 1025 °C. The melt was cooled and dissolved in a nitric, hydrochloric and hydrofluoric acid mixture and diluted for ICP-MS to determine trace element content. Standard sample JG-2 was used to detect the reliability of analytical results with errors for major elements and most trace elements of about 1–5% and 5–10%, respectively.

4. Results

Major element compositions of the skarns from the Huangshaping, Shizhuyuan and Xianghualing deposits are presented in Table S1, and trace element compositions are given in Tables S2–S4. Previously published geochemical data on these skarns are discussed. The loss-on-ignition (LOI) for most samples was <10 wt %. The skarns from the three deposits are characterized by variable chemical compositions, notably for SiO_2, Al_2O_3, total Fe, MgO and CaO. The oxides vary between deposits too, with the Huangshaping skarn displaying the widest ranges of SiO_2 (28.77–87.18%), total Fe (0.98–46.25%), MgO (0.09–20.07%), CaO (1.33–37.78%), Na_2O (0.03–3.95%) and K_2O (0.12–6.88%), the Shizhuyuan skarn showing the most variable MnO contents (0.12–2.46%), the Xianghualing skarn yielding the widest range of Al_2O_3 (2.89–21.06%), TiO_2 (<0.01–1.11%) and P_2O_5 (0.01–0.20%), respectively (Figure 6a–i). When comparing the compositional range of skarns with those of skarn-related granites and host sedimentary strata, the Huangshaping skarn is characterized by a relatively wide elemental distribution, with only a few samples plotting around or within the granite range, while other samples plot close to the range defined by the host strata. By contrast, the Shizhuyuan skarn has a relatively narrow range of major elements that corresponds most closely to sedimentary strata. In addition, the SiO_2 contents of skarn samples from different deposits show distinct linear trends with other oxides, such as Al_2O_3, total Fe, MnO and CaO (Figure 6).

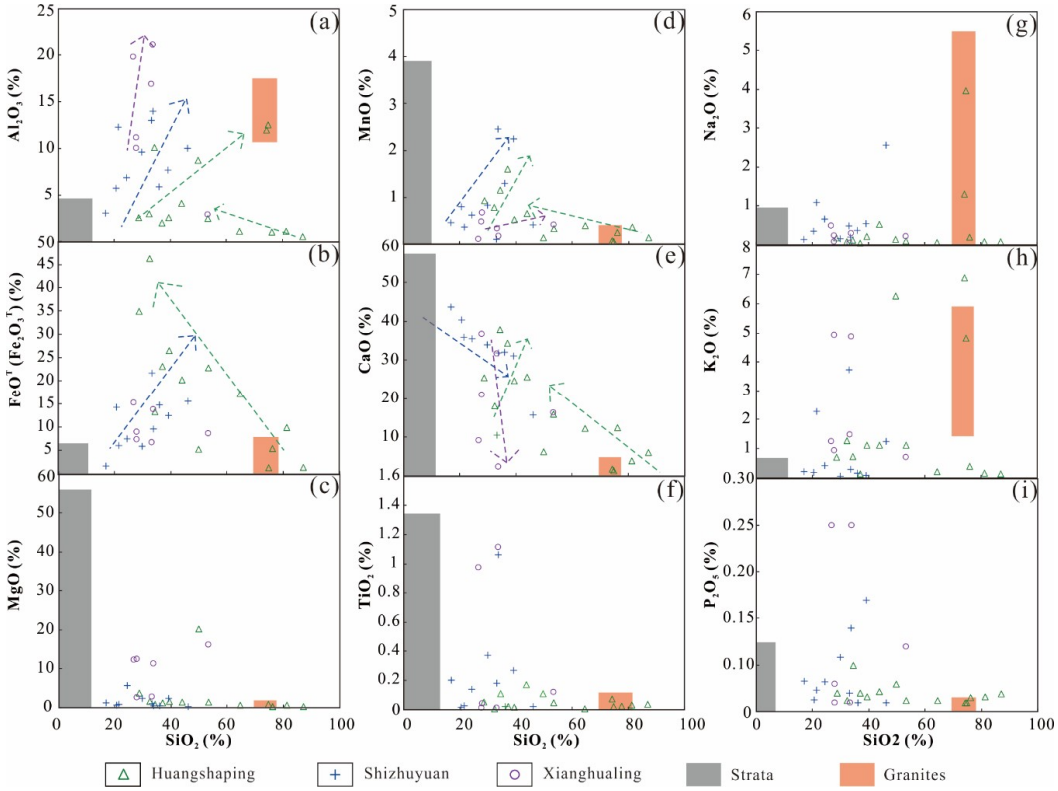

Figure 6. Correlation plots of skarn oxide compositions, compared to those of granites and strata of the Huangshaping, Shizhuyuan and Xianghualing deposits. (**a**) SiO_2 vs. Al_2O_3 diagram; (**b**) SiO_2 vs. FeO^T ($Fe_2O_3{}^T$) diagram; (**c**) SiO_2 vs. MgO diagram; (**d**) SiO_2 vs. MnO diagram; (**e**) SiO_2 vs. CaO diagram; (**f**) SiO_2 vs. TiO_2 diagram; (**g**) SiO_2 vs. Na_2O diagram; (**h**) SiO_2 vs. K_2O diagram and (**i**) SiO_2 vs. P_2O_5 diagram. Colored arrows show correlation trends for skarns (color coded to match data points). The orange box shows the range of composition of granites from all three deposits. The gray box shows the composition of the Carboniferous limestone at Huangshaping and Devonian limestone at other deposits in the Nanling range. No strata analysis was available at the Shizhuyuan and Xianghualing deposits. Data for the granites are reference from [24,44,68,76]. Data for the strata are from [31,77].

Likewise, the trace element compositions of all skarn samples are also highly variable (Figure 7a–i). The Xianghualing skarn has the highest enrichments of LILE such as Ba (10.1–1045 ppm), Rb (139.5–2440 ppm) and Cs (14.8 to 610 ppm), followed by the Huangshaping and Shizhuyuan skarns. In addition, Sr is extremely enriched in the Shizhuyuan skarn (20.4–680 ppm), followed by the Xianghualing (20.1–154 ppm) and Huangshaping (6.8–99.6 ppm) skarns. Regarding the HFSE, the Huangshaping skarn contains the most variable contents of Nb (0.30–88.2 ppm), Hf (0.2–28.3 ppm) and Th (0.82–48 ppm), respectively. The Xianghualing skarn has the highest Zr (up to 534 ppm) and U (up to 90.3 ppm) concentrations, followed by the Shizhuyuan (up to 365 and 36.7 ppm, respectively) and Huangshaping skarns (up to 130 and 32 ppm, respectively). On primitive mantle-normalized spider diagrams (Figure 8a–c), the Huangshaping skarn samples are strongly depleted in Ti, but enriched in Hf, while the Shizhuyuan skarn samples show moderate values for most elements. The weakest Ba anomaly and most significant U anomalies are recorded in the Xianghualing skarn. By comparing skarn compositions with the associated granite and sedimentary strata, it can be concluded that the Huangshaping skarn is most closely related to the granite, whereas the Shizhuyuan skarn seems to be more similar to regional strata in terms of its trace element composition.

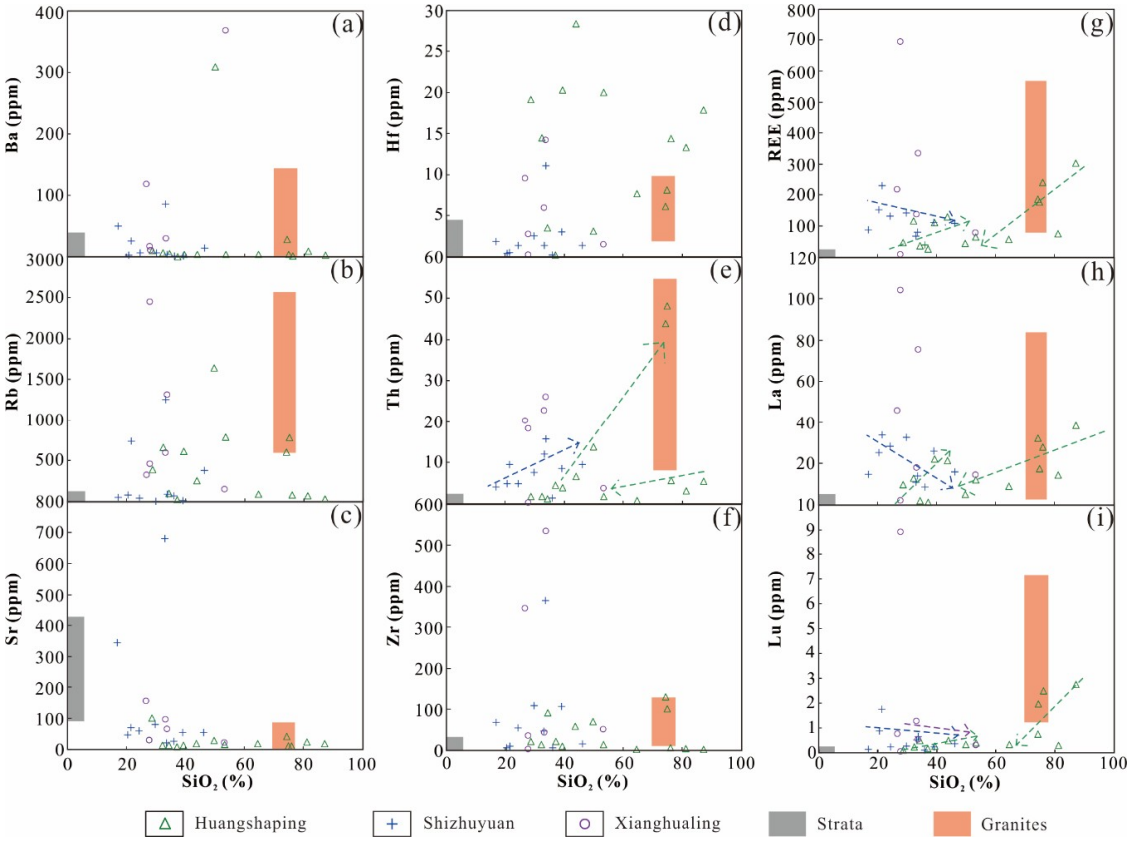

Figure 7. Correlation plots of trace elements vs. SiO_2 in skarns. Colored arrows show correlation trends for skarns (color coded to match data points). (**a**) SiO_2 vs. Ba diagram; (**b**) SiO_2 vs.Rb diagram; (**c**) SiO_2 vs. Sr diagram; (**d**) SiO_2 vs. Hf diagram; (**e**) SiO_2 vs. Th diagram; (**f**) SiO_2 vs. Zr diagram; (**g**) SiO_2 vs. REE diagram; (**h**) SiO_2 vs. La diagram and (**i**) SiO_2 vs. Lu diagram. The orange box shows the range of composition of granites from all three deposits. The box shows the composition of the Carboniferous limestone at Huangshaping and Devonian limestone at other deposits in the Nanling range. No strata analysis was available at the Shizhuyuan and Xianghualing deposits. Data sources for the granites and strata are the same as in Figure 6.

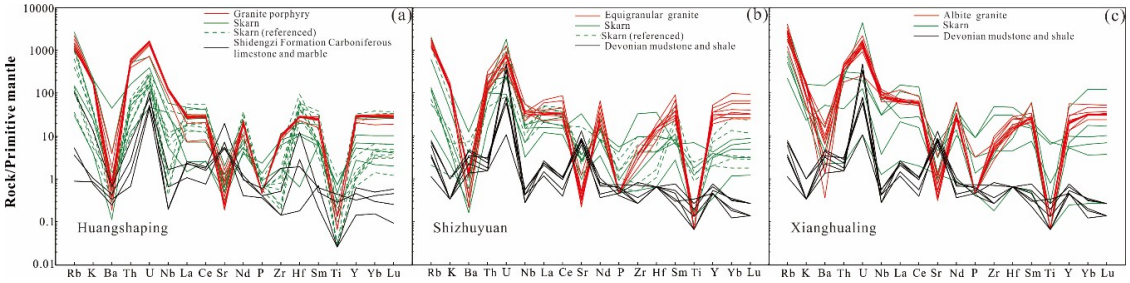

Figure 8. Primitive mantle-normalized trace element diagrams for granites, strata and skarns from the (**a**) Huangshaping, (**b**) Shizhuyuan and (**c**) Xianghualing deposit. Skarn data are from this study, and are reference from [25,31]. Strata composition of the Shidengzi Formation Carboniferous limestone are reference from [31], Devonian mudstone and shale composition are reference from [77]. Granite composition of the Huangshaping granite porphyry are reference from [24], Shizhuyuan equigranular biotite granite are reference from [44,68], Xianghualing albite granite are reference from [76]. Normalized values for primitive mantle are from [78].

The rare earth elements (REE) of three skarn samples are characterized by variable total REE contents and fractionation between LREE and HREE (Figure 9a–c). The Xianghualing skarn samples have the most variable and highest total REE contents (up to 693.5 ppm), with high La (1.8–104 ppm), Ce (3.5–245 ppm) (Figure 7g–i) and Yb (0.13–60.2 ppm). The average total REE content of the Huangshaping and Shizhuyuan skarns is lower. In addition, the fractionation between LREE and HREE in the Shizhuyuan skarn (highest average $(La/Yb)_N = 7.7$) is stronger than that at the Huangshaping and Xianghualing skarns (Figure 9). The negative Eu anomaly in the Xianghualing skarn samples is the weakest and shows a similar REE pattern to its hosted granite. By contrast, the Huangshaping skarn samples have the largest Eu anomalies, which are also similar to its parent granite (Figure 9a).

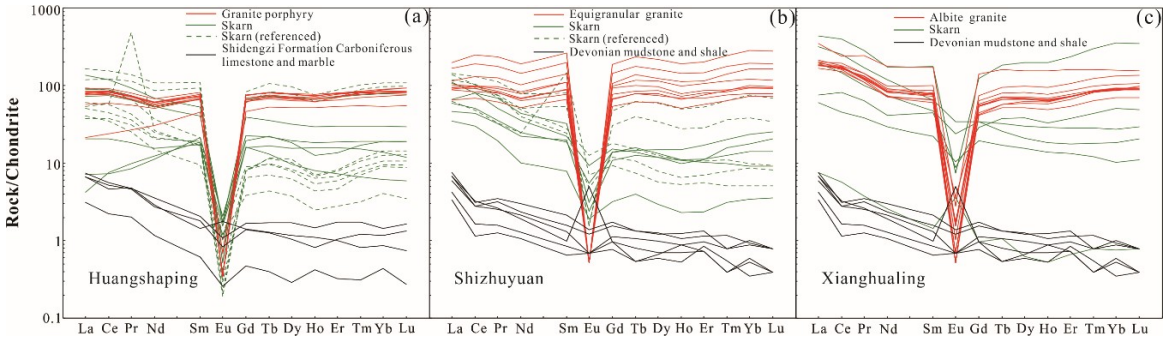

Figure 9. Chondrite-normalized REE patterns for granites, strata and skarns of the (**a**) Huangshaping, (**b**) Shizhuyuan and (**c**) Xianghualing deposits. Data sources are the same as in Figure 8. Normalized values for chondrite are from [78].

5. Discussion

5.1. Magma Differentiation and Metasomatism

The skarns at the Huangshaping, Shizhuyuan and Xianghualing deposits are located at the contact zones between granitic intrusions and strata (mainly carbonate rocks) (Figures 2–4). This reflects the undisputed role of granites in the formation of skarns. It is important to examine the differences in magma composition of the skarn-related granites at each deposit and to assess the possible impact on the respective metal contents.

The skarn-related granites in the three deposits are highly differentiated and can be classified as reduced, high-K-calc-alkaline, A_2-subtype granitoids, formed in an extensional tectonic setting [24,33,34,44,63,68].

In addition, the granites are believed to have contributed a large proportion of the volatile components (especially fluorine, [24,25,36,42,44,62,68,72]) and ore-forming elements [16,40,47,52]. Although the parental magmas of the three granitic plutons are highly fractionated, the degree of differentiation, which can be inferred from whole-rock element compositions, could vary between the plutons. In general, the Rb content will increase with increasing degree of differentiation, whereas Ba and Sr are usually enriched in the early stage during magmatic evolution without an obvious variation of K. This means that K/Rb and Rb/Sr ratios can be used to evaluate the degree of fractionation of the magmas [24,79,80]. The Xianghualing granite has the lowest K/Rb ratio (mean = 22), but the highest Rb/Sr ratio (mean = 146.9), indicating that it is the most differentiated (Table S5, [81]). Moreover, the Laiziling pluton (i.e., the Xianghualing granite) can be divided into several magmatic-hydrothermal zones from the base to the top [73], also suggesting strong crystal fractionation. On the other hand, previous studies reveal that the Huangshaping granite porphyry is coarse-grained and porphyritic in texture, and crystallized over an extended period (~10 Myr; [82]) and at a high crystallization temperatures (~915 °C; [34]). This contrasts with the relatively low crystallization temperatures (680–725 °C) for both the Shizhuyuan and Xianghualing granite which have a hypidiomorphic granular texture [33,68]. In summary, the Xianghualing granite appears to exhibit the strongest degree of magma differentiation, followed by the Huangshaping granite and finally, the Shizhuyuan granite.

By comparing the compositions of the skarns with the composition of the associated granites and sedimentary strata, it is evident that the Huangshaping skarn, which can be classified as a siliceous skarn, has the most variable elemental composition, and one that shows affinities to both the granite and strata compositions (Figures 6 and 7), probably indicating varied protoliths of the skarn components. The average content of Si in the Huangshaping skarn is much higher than those in other skarns. This may imply that Si was sourced from the highly evolved granite in this deposit. Due to the very low abundances of both Si and Al in the host strata (Table S6), the migration or exchange of these two elements between two end members (granites and strata) is probably mainly controlled by fluids derived from the granites. Both the Shizhuyuan and Xianghualing skarns exhibit positive correlations between Al, Mn and Ca oxides and SiO_2, whereas the Huangshaping skarns show two opposite trends (see arrows in Figure 6a,d,e), indicating contributions from both the granites and strata. The negative correlation between SiO_2 and CaO in the Shizhuyuan and Xianghualing skarns can be attributed to their protolith properties (carbonate rocks). Highly differentiated magma-related fluids may provide strong exchange capacity and thus mobilize these major elements.

The average Al_2O_3 content in the skarns show a decreasing trend from Xianghualing (average = 13.62%) to Shizhuyuan (average = 8.80%) and then to Huangshaping (average = 4.54%), which is inconsistent with other oxides. This may indicate that the Xianghualing skarn inherited most of its metal elements from the granite. By contrast, this effect is less pronounced at the Huangshaping and Shizhuyuan skarns, respectively. It is also reasonable to speculate that the activity of Al was suppressed by the gradual enrichment of Fe during metasomatism (Table S5). This is evidenced by the gradation of garnet types from grossular to almandine with increasing metasomatism, and the dominant pyroxene composition being hedenbergite [35].

Trace element contents may also reflect variations in the granite composition of the studied skarns. Some trace elements, such as Ba, Rb, Cr, Cs, V, Ga and most REEs, are enriched in skarns and in the associated granites, especially in the Xianghualing samples (Table S6). This implies the dominant control of granites on these elements during metasomatism. Although the average contents of other trace elements (such as Nb, Y, Zr, Th and U) in skarns are lower than those of granites, their maximum values are comparable to as those in granites. This further suggests that granites influenced the enrichment of those trace elements in the skarns. Moreover, consistent linear trends for these skarns can be observed on the Zr vs. Hf, Ba vs. Sr, Zr vs. Ti and U vs. Th diagrams (Figure 10), probably indicating that these elements may actived in pairs during metasomatism, aided by the intrusion of granites. In addition, the two distinct and contrasting trends of the Huangshaping skarn on the Zr vs. Ti diagram (green arrows, Figure 10c) indicates at least two types of skarns in this area.

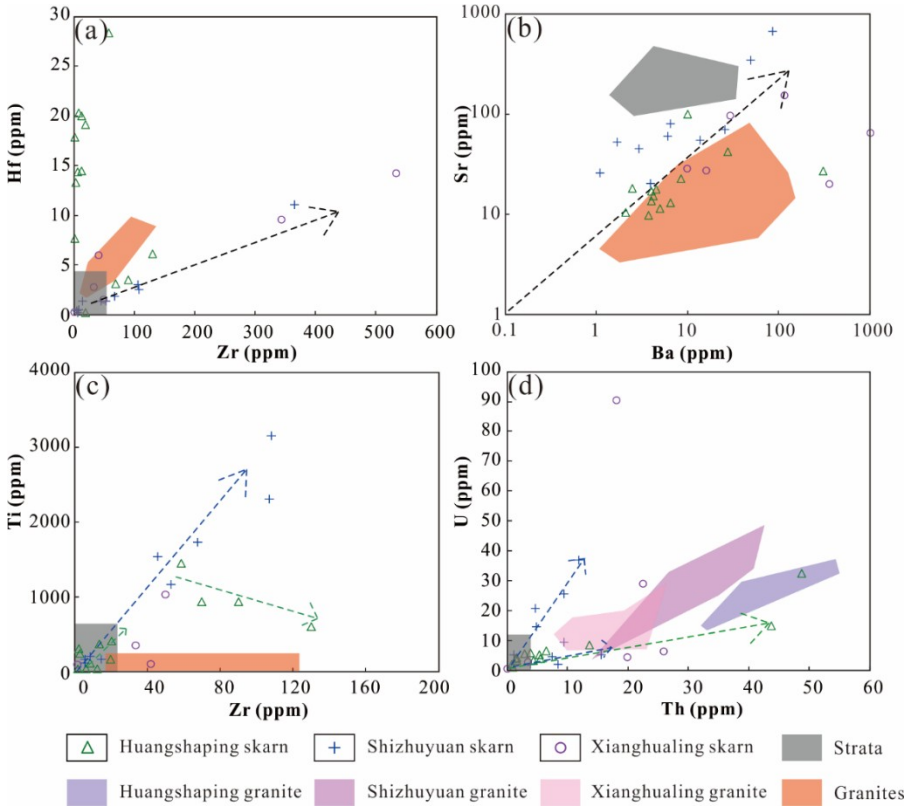

Figure 10. Correlation of trace elements in skarns, illustrating the geochemical behavior of typical trace elements during metasomatism. (**a**) Zr vs. Hf diagram; (**b**) Ba vs. Sr diagram; (**c**) Zr vs. Ti diagram and (**d**) Th vs. U diagram. The colored arrows are provided to highlight correlation trends (black arrow shows overall trend for all skarns, with the green arrow for Huangshaping and blue arrow for Shizhuyuan). The orange box shows the range of composition of all granites from the three deposits and the gray box shows the range of composition of the Carboniferous limestone at Huangshaping and Devonian limestone at other deposits in the Nanling range. Data sources are the same as in Figure 8.

In summary, the Xianghualing skarn composition is most strongly influenced by the parent granite composition, by contrast, this effect is less pronounced at the Shizhuyuan and Huangshaping skarns, respectively. Major elements such as Si and Al, and most trace elements such as Ba, Rb, Cs, Cr, V, Ga, Nb, Zr, U and Th in the skarns are dominantly controlled by the composition of the related granites.

5.2. Strata Contribution to Skarns

The sedimentary strata also has an impact on the composition of skarns. The mean total FeO content of the skarns is 16.26%, 10.86% and 10.02% at Huangshaping, Shizhuyuan and Xianghualing, respectively (Table S5). These Fe contents can be can be primarily ascribed to stratigraphic fluids released from host sediments or regional strata, due to the very low contents of Fe in the three related granites. High contents of CaO (43.62%) and MgO (20.07%) in the skarns may stem from the carbonate rocks at each deposit, and the similarity of MnO and TiO_2 contents in skarns and strata indicate that such components are dominantly inherited from the local strata (Figure 6d,f).

The Sr contents are relatively high in both the sedimentary strata and skarns (average = 143.3 ppm) at Shizhuyuan (Table S6), indicating the dominant role of strata in Sr enrichment. The ∑REE content varies widely within individual skarns, especially at Xianghualing where the ∑REE content ranges from 8.0 to 693.5 ppm, also suggesting the combined control of both granite and strata on its composition at this site. The ratios of $(LREE/HREE)_T$ (6.1 to 8.4) and $(La/Yb)_N$ (3.8 to 7.7) in skarns are also in accordance with the average ratios of the strata. Moreover, the steepness of the REE pattern from

LREE to HREE at both Shizhuyuan and Xianghualing is more similar to the parent strata than the corresponding granite on chondrite-normalized REE diagrams (Figure 9), suggesting that the host strata influenced the REE signatures of the skarns. By contrast, the REE pattern of the Huangshaping skarn can be classified into two types: (1) one shows a steep REE pattern and significant negative Eu anomaly, similar to that of the parent granite; and (2) the other shows a shallower REE pattern and a moderate Eu anomaly, reflecting control by both granite and strata. The REE contents of most skarns moderately decrease along with increasing SiO_2, except for some Huangshaping samples which show the opposite trend for La and Lu (Figure 7h,i). All of this could imply varied protoliths of the Huangshaping skarn.

In summary, the REE signatures of the Shizhuyuan and Xianghualing skarns are more strongly influenced by the sedimentary strata, while the REE signatures at the Huangshaping skarn suggest influence of both strata and granite. Major elements such as Fe, Mn, Mg and Ca in the skarns are dominated by the host sedimentary strata, and Sr and REE patterns are mainly inherited from the surrounding sedimentary rocks.

5.3. Source of Metals and Scales of Skarn Mineralization

As described below, numerous previous studies have focused on the temperature, pressure, crystallization depth and ore-forming relationships in the skarns at the Huangshaping, Shizhuyuan and Xianghualing deposits. For the Huangshaping skarn, two crystallization stages (>500 °C and 250–476 °C, respectively) are distinguished [32]. Homogenization temperatures of fluid inclusions in the Shizhuyuan skarn minerals range from 350 °C to 535 °C [28]. Based on the analysis of hessonite inclusions, the formation temperature of the Xianghualing skarn is estimated to be 430–570 °C [29]. Thus, the diagenetic pressures are estimated to be 0.2–0.85 kbar at Huangshaping [32,83], 1.8–3.2 kbar at Shizhuyuan [30] and 0.2–1.0 kbar at Xianghualing [29], corresponding to the formation depth of skarns and related mineralization at 0.7–3.0 km for Huangshaping, 5.4–12 km for Shizhuyuan, and 0.7–3.5 km for Xianghualing. In summary, the Shizhuyuan skarns formed under the highest temperatures and pressures and the deepest formation depth, consistent with most W skarns (formation depth of 5–20 km; [84]. Consequently, it can be inferred that the precipitation of multiple metals (especially W) in the Shizhuyuan area occurred in a deep, high-pressure setting, in which magma differentiation was largely suppressed. By contrast, local strata composition strongly influenced skarn formation and mineralization.

Skarn mineralization in the Nanling Range can be divided into three types in terms of dominant mineralization element: (1) the Huangshaping W–Mo–Sn; (2) Shizhuyuan W–Sn–Mo–Bi; and (3) the Xianghualing Sn. The W skarns are closely related to calc-alkaline plutons and can be further divided into reduced and oxidized types [4]. The reduced type W skarns are composed of hedenbergite, grandite garnet and low-molybdenum scheelite in the early stages. During the later stages, garnet is subcalcic, and dominated by spessartine and almandine. Moreover, enrichment of W is likely to be favored by reduced environments and under more reduced conditions, there is strong affinity between W and Sn [85]. The Sn skarn is closely related to high-silica magma under reducing conditions [4]. For the W–Mo–Cu assemblage, a reducing environment with high fluorine is favored. Therefore, it can be concluded that reducing environments were dominated in the skarn mineralization in the Nanling Range, with an increasing reduction states from the Xianghualing Sn to the Huangshaping W–Mo–Sn and then to the Shizhuyuan W–Sn–Mo–Bi deposit. The abundant Bi contents in the Shizhuyuan skarn may be attributed to the strong influence of the sedimentary wall rocks at Shizhuyuan.

As discussed above, the Xianghualing and Huangshaping skarns have a greater affinity to their strongly differentiated parent granites, compared to the Shizhuyuan skarn which has strong affinities to the host sediments. The Xianghualing granite is the most evolved, enriching in most trace elements (e.g., Ba, Rb, Cr, Cs, V, Ga and most REEs), and its related skarn is also the richest. However, Sn is the only ore-forming element at Xianghualing and metal reserves are relatively low compared to the W–Mo–Sn skarn at Huangshaping. Compared to the Xianghualing and Huangshaping skarns,

the Shizhuyuan skarn is characterized by the largest ore-forming scale, most varied mineral species and smallest pluton size (~10 km^2). It is interesting that such a small pluton contributed to the formation of a giant polymetallic deposit. There are many similarities between these three deposits, such as well-developed structures and multiphase magmatic-hydrothermal activity. We suggest that strongly evolved granites (e.g., the Xianghualing granite) may be less favorable for the development of mineralization, hence, resulting in a relatively small size of deposits. By contrast, less differentiated, smaller plutons formed at greater depths (e.g., the Shizhuyuan granite) may favor the formation of mineralized skarns where substantial amount of ore-forming metals stems from host sedimentary strata. The sedimentary rocks at Shizhuyuan have high concentrations of metals (average W contents of 5–6 ppm and average Sn contents of 2–8 ppm) [86], and the hot environment resulting from deep magmatic activity probably creating suitable conditions for widespread fluid convection in the sedimentary strata as well as strong water-rock interaction [70]. Although the abundance of ore metals in the strata could be lower than in the granite, fluid circulation through a large volume of strata may concentrate these elements more effectively than a limited volume of granite. The Shizhuyuan deposit was less influenced by granite-derived fluids due to the relatively low degree of differentiation of the magma; however, continuous magmatic activity and an extended hot environment likely accounted for the prolonged circulation of stratigraphic fluids. These fluids carried ore-forming elements through fractures widely developed in the deposit area, constantly assimilating ore-forming material from surrounding strata, and eventually forming the giant Shizhuyuan skarn deposits (Figure 11). By contrast, the Xianghualing granite experienced the strongest degree of magmatic differentiation, resulting in relatively low abundance and a single element (Sn) skarn mineralization with a minor contribution from the strata. The metasomatism and mineralization at Xianghualing has more affinities with local magmatism. At Huangshaping deposit, both granite and strata may equally have contributed in forming the W–Mo–Sn mineralization (Figure 11).

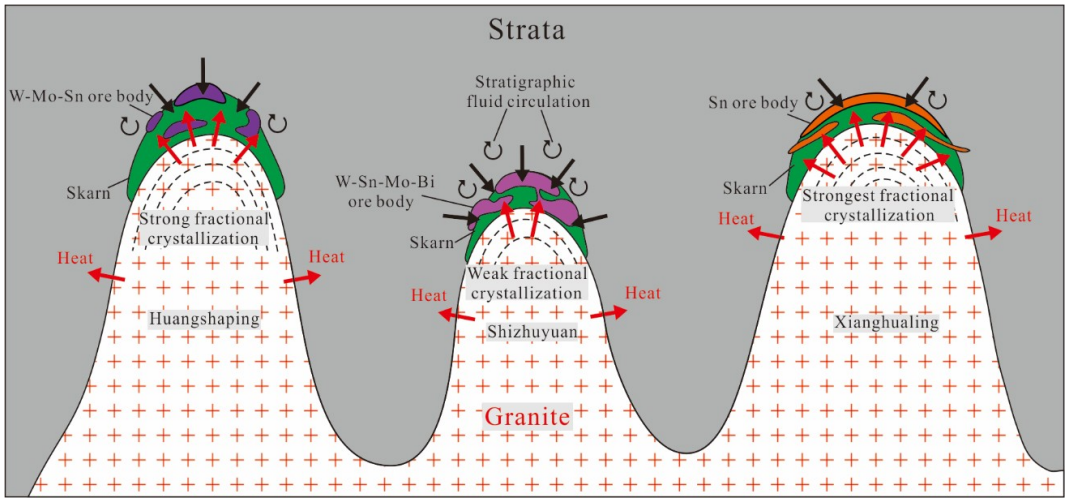

Figure 11. A genetic model for W–Sn polymetallic skarn deposits in the Nanling Range, South China, showing relative material contributions from granite and strata, respectively.

6. Conclusions

(1) Concentrations of Si, Al and most trace elements (e.g., Ba, Rb, Cs, Cr, V, Ga, Nb, Zr, U and Th) in ore-related skarns controlled by related granites but FeO, CaO, MgO, MnO, TiO_2, Sr and REE signatures in most skarns are significantly controlled by the composition of the host sediments. The composition of strata plays a crucial role in the enrichment of polymetallic elements, scale and metallogenic ore species of the W–Sn skarn mineralization in South China.

(2) The formation of the Shizhuyuan W–Sn–Mo–Bi polymetallic skarn deposit is strongly controlled by strata during metasomatism. The Xianghualing Sn skarn is controlled by the granite composition. Granite and strata may have contributed almost equally to the Huangshaping W–Mo–Sn deposit, however.

Supplementary Materials: The following are available online at http://www.mdpi.com/2075-163X/8/7/265/s1, Table S1: Major element compositions of skarns from the Huangshaping, Shizhuyuan and Xianghualing deposit (%), Table S2: Trace element compositions of skarns in the Huangshaping deposit (ppm), Table S3: Trace element compositions of skarns in the Shizhuyuan deposit (ppm), Table S4: Trace element compositions of skarns in the Xianghualing deposit (ppm), Table S5: Minimum, maximum and average values of trace element compositions in skarns, granites and strata (ppm), Table S6: Minimum, maximum and average values of major element compositions in skarns, granites and strata (%).

Author Contributions: H.L., W.J. and J.W. conceived and designed the experiments; H.L., W.J., J.W. and J.C. took part in the field investigation; W.J., H.L. and N.J.E. interpreted the data and took part in the discussion; W.J. wrote the original draft; H.L. and N.J.E. reviewed and edited the paper.

Funding: This work was funded by the National Natural Science Foundation of China (Grant Nos. 41502067).

Acknowledgments: The authors are thankful to Hua Kong, Qilin Peng and Yong Wang for their kind cooperation during the fieldwork. The authors are also grateful to the editorial board members and other two reviewers for their constructive comments that greatly improved this manuscript.

Conflicts of Interest: The authors declare no conflict of interest.

References

1. Einaudi, M.T.; Meinert, L.D.; Newberry, R.J. Skarn deposits. *Econ. Geol.* **1981**, *964*, 317–391.
2. Einaudi, M.T.; Burt, D.M. Introduction-terminology, classification, and composition of skarn deposits. *Econ. Geol.* **1982**, *77*, 745–754. [CrossRef]
3. Mueller, A.G. The Savage Lode magnesian skarn in the Marvel Loch gold–silver mine, Southern Cross greenstone belt, Western Australia. Part 1: Structural setting, petrography, and geochemistry. *Can. J. Earth Sci.* **1991**, *28*, 659–685. [CrossRef]
4. Meinert, L.D. Skarns and skarn deposits. *Geosci. Can.* **1992**, *19*, 145–162.
5. Jamtveit, B.; Wogelius, R.A.; Fraser, D.G. Zonation patterns of skarn garnets: Records of hydrothermal system evolution. *Geology* **1993**, *21*, 113–116. [CrossRef]
6. Gaspar, M.; Knaack, C.; Meinert, L.D.; Moretti, R. REE in skarn systems: A LA-ICP-MS study of garnets from the Crown Jewel gold deposit. *Geochim. Cosmochim. Acta* **2008**, *72*, 185–205. [CrossRef]
7. Ismail, R.; Ciobanu, C.L.; Cook, N.J.; Teale, G.S.; Giles, D.; Mumm, A.S.; Wade, B. Rare earths and other trace elements in minerals from skarn assemblages, Hillside iron oxide–copper–gold deposit, Yorke Peninsula, South Australia. *Lithos* **2014**, *184–187*, 456–477. [CrossRef]
8. Alirezaei, S.; Einali, M.; Jones, P.; Hassanpour, S.; Arjmandzadeh, R. Mineralogy, geochemistry, and evolution of the Mivehrood skarn and the associated pluton, northwest Iran. *Int. J. Earth Sci.* **2015**, *105*, 849–868. [CrossRef]
9. Hu, X.L.; Gong, Y.J.; Pi, D.H.; Zhang, Z.J.; Zeng, G.P.; Xiong, S.F.; Yao, S.Z. Jurassic magmatism related Pb–Zn–W–Mo polymetallic mineralization in the central Nanling Range, South China: Geochronologic, geochemical, and isotopic evidence from the Huangshaping deposit. *Ore Geol. Rev.* **2017**, *91*, 877–895. [CrossRef]
10. Yin, S.; Ma, C.Q.; Xu, J.N. Geochronology, geochemical and Sr–Nd–Hf–Pb isotopic compositions of the granitoids in the Yemaquan orefield, East Kunlun orogenic belt, northern Qinghai-Tibet Plateau: Implications for magmatic fractional crystallization and sub-solidus hydrothermal alteration. *Lithos* **2017**, *294–295*, 339–355. [CrossRef]
11. Chen, J.; Halls, C.; Stanley, C.J. Rare earth element contents and patterns in major skarn minerals from Shizhuyuan W, Sn, Bi and Mo deposit, South China. *Geochem. J.* **1992**, *26*, 147–158. [CrossRef]
12. Giuliani, G.; Cheilletz, A.; Mechiche, M. Behaviour of REE during thermal metamorphism and hydrothermal infiltration associated with skarn and vein-type tungsten ore bodies in central Morocco. *Chem. Geol.* **1987**, *64*, 279–294. [CrossRef]

13. Ma, W.; Liu, Y.C.; Yang, Z.S.; Li, Z.Q.; Zhao, X.Y.; Fei, F. Alteration, mineralization, and genesis of the Lietinggang–Leqingla Pb–Zn–Fe–Cu–Mo skarn deposit, Tibet, China. *Ore Geol. Rev.* **2017**, *90*, 897–912. [CrossRef]
14. Siesgesmund, S.; López-Doncel, R.; Sieck, P.; Wilke, H.; Wemmer, K.; Frei, D.; Oriolo, S. Geochronological and geochemical constraints on the genesis of Cu-Au skarn deposits of the Santa María de la Paz district (Sierra del Fraile, Mexico). *Ore Geol. Rev.* **2018**, *94*, 310–325. [CrossRef]
15. Baker, J.H.; Hellingwerf, R.H. Rare earth element geochemistry of W-Mo-(Au) skarns and granites from Western Bergslagen, central Sweden. *Miner. Petrol.* **1988**, *39*, 231–244. [CrossRef]
16. Hua, R.M.; Chen, P.R.; Zhang, W.L.; Junming, Y.; Lin, J.F.; Zhang, Z.S.; Gu, S.Y.; Liu, X.D.; Qi, H.W. Metallogenesis related to Mesozoic granitoids in the Nanling Range, South China and their geodynamic settings. *Acta Geol. Sin-Engl. Ed.* **2005**, *79*, 810–820.
17. Mao, J.W.; Xie, G.Q.; Guo, C.L.; Chen, Y.C. Large scale tungsten-tin mineralization in the Nanling region, South China: Metallogenic ages and corresponding geodynamic processes. *Acta Petrol. Sin.* **2007**, *23*, 2329–2338. (In Chinese)
18. Cao, J.Y.; Wu, Q.H.; Yang, X.Y.; Kong, H.; Li, H.; Xi, X.S.; Huang, Q.F.; Liu, B. Geochronology and Genesis of the Xitian W-Sn Polymetallic Deposit in Eastern Hunan Province, South China: Evidence from Zircon U-Pb and Muscovite Ar-Ar Dating, Petrochemistry, and Wolframite Sr-Nd-Pb Isotopes. *Minerals* **2018**, *8*, 111. [CrossRef]
19. Jiang, W.C.; Li, H.; Wu, J.H.; Zhou, Z.K.; Kong, H.; Cao, J.Y. A newly found biotite syenogranite in the Huangshaping polymetallic deposit, South China: Insights into Cu mineralization. *J. Earth Sci.* **2018**. [CrossRef]
20. Yang, J.H.; Kang, L.F.; Peng, J.T.; Zhong, H.; Gao, J.F.; Liu, L. In-situ elemental and isotopic compositions of apatite and zircon from the Shuikoushan and Xihuashan granitic plutons: Implication for Jurassic granitoid-related Cu-Pb-Zn and W mineralization in the Nanling Range, South China. *Ore Geol. Rev.* **2018**, *93*, 382–403. [CrossRef]
21. Lu, Y.F.; Ma, L.Y.; Qu, W.J.; Mei, Y.P.; Chen, X.Q. U-Pb and Re-Os isotope geochronology of Baoshan Cu–Mo polymetallic ore deposit in Hunan Province. *Acta Petrol. Sin.* **2006**, *22*, 2483–2492. (In Chinese)
22. Peng, J.T.; Zhou, M.-F.; Hu, R.Z.; Shen, N.P.; Yuan, S.D.; Bi, X.W.; Du, A.D.; Qu, W.J. Precise molybdenite Re–Os and mica Ar–Ar dating of the Mesozoic Yaogangxian tungsten deposit, central Nanling district, South China. *Miner. Depos.* **2006**, *41*, 661–669. [CrossRef]
23. Yuan, S.D.; Peng, J.T.; Hu, R.Z.; Li, H.M.; Shen, N.P.; Zhang, D.L. A precise U–Pb age on cassiterite from the Xianghualing tin-polymetallic deposit (Hunan, South China). *Miner. Depos.* **2007**, *43*, 375–382. [CrossRef]
24. Li, H.; Watanabe, K.; Yonezu, K. Geochemistry of A-type granites in the Huangshaping polymetallic deposit (South Hunan, China): Implications for granite evolution and associated mineralization. *J. Asian Earth Sci.* **2014**, *88*, 149–167. [CrossRef]
25. Cheng, Y.S. Petrogenesis of skarn in Shizhuyuan W-polymetallic deposit, southern Hunan, China: Constraints from petrology, mineralogy and geochemistry. *Trans. Nonferr. Met. Soc. China* **2016**, *26*, 1676–1687. [CrossRef]
26. Ye, Z.H.; Wang, P.; Xiang, X.K.; Wang, A.J.; Yan, Q.; Li, Y.K. Re-Os dating and H-O isotope geochemistry of the Shimensi deposit, northern Jiangxi, China: Implication for ore genesis. *Geochem. J.* **2016**, *50*, 139–152. [CrossRef]
27. Liu, J.P. Indium Mineralization in a Sn-Poor Skarn Deposit: A Case Study of the Qibaoshan Deposit, South China. *Minerals* **2017**, *7*, 76. [CrossRef]
28. Lu, H.Z.; Liu, Y.M.; Wang, C.L.; Xu, Y.Z.; Li, H.Q. Mineralization and fluid inclusion study of the Shizhuyuan W–Sn–Bi–Mo–F skarn deposit, Hunan Province, China. *Econ. Geol.* **2003**, *98*, 955–974. [CrossRef]
29. Zhou, T. *Research on the Geochemistry and Thermodynamics Characteristics in Xianghualing Mining Area in Hunan Province*; Central South University: Changsha, China, 2009. (In Chinese)
30. Cheng, X.Y. *Research on the Skarns Formation Mechanism of the Shizhuyuan W–Sn Polymetallic Deposit, Hunan Province*; Kunming University of Science and Technology: Kunming, China, 2012. (In Chinese)
31. Qi, F.Y.; Zhang, Z.; Zhu, X.Y.; Li, Y.S.; Zhen, S.M.; Gong, F.Y.; Gong, X.D.; He, P. Skarn geochemistry of the Huangshaping W–Mo polymetallic deposit in Hunan and its geological significance. *Geol. China* **2012**, *39*, 338–348. (In Chinese)

32. Huang, C.; Li, X.F.; W, L.F.; Liu, F.P. Fluid inclusion study of the Huangshaping polymetallic deposit, Hunan Province, South China. *Acta Petrol. Sin.* **2013**, *29*, 4232–4244. (In Chinese)
33. Lai, S.H. *Research on Mineralization of the Xianghualing Tin Polymetallic Deposit, Hunan Province, China*; China University of Geoscience: Beijing, China, 2014. (In Chinese)
34. Yuan, Y.B. *The Genetic Difference between Two Metallogenic Granites and the Ore-Forming Material Source of the Huangshaping Deposit in Southern Hunan*; China University of Geoscience: Beijing, China, 2015. (In Chinese)
35. Zhao, F.; Yin, J.W.; Wang, M.Y.; Zhang, Z.H.; Sun, Y.D.; Zhang, P.; Gao, Y.W.; Wang, L.F.; Zong, Z.H. Skarn mineral characteristics and their geological significance of the Huangshaping deposit in Hunan Province. *Geoscience* **2016**, *30*, 1038–1050. (In Chinese)
36. Liu, J.P.; Rong, Y.N.; Zhang, S.G.; Liu, Z.F.; Chen, W.K. Indium Mineralization in the Xianghualing Sn-Polymetallic Orefield in Southern Hunan, Southern China. *Minerals* **2017**, *7*, 173. [CrossRef]
37. Liu, J.P.; Rong, Y.N.; Gu, X.P.; Shao, Y.J.; Lai, J.Q.; Chen, W.K. Indium Mineralization in the Yejiwei Sn-Polymetallic Deposit of the Shizhuyuan Orefield, Southern Hunan, China. *Resour. Geol.* **2018**, *68*, 22–36. [CrossRef]
38. Wang, Y.J.; Fan, W.M.; Guo, F. Geochemistry of early Mesozoic potassium-rich diorites-granodiorites in southeastern Hunan Province, South China: Petrogenesis and tectonic implications. *Geochem. J.* **2003**, *37*, 427–448. [CrossRef]
39. Shu, X.J.; Wang, X.L.; Sun, T.; Xu, X.S.; Dai, M.N. Trace elements, U–Pb ages and Hf isotopes of zircons from Mesozoic granites in the western Nanling Range, South China: Implications for petrogenesis and W–Sn mineralization. *Lithos* **2011**, *127*, 468–482. [CrossRef]
40. Mao, J.W.; Cheng, Y.B.; Chen, M.H.; Pirajno, F. Major types and time–space distribution of Mesozoic ore deposits in South China and their geodynamic settings. *Miner. Depos.* **2013**, *48*, 267–294. [CrossRef]
41. Zhu, X.Y.; Wang, J.B.; Wang, Y.L.; Cheng, X.Y.; Fu, Q.B. Sulfur and lead isotope constraints on ore formation of the Huangshaping W–Mo–Bi–Pb–Zn polymetallic ore deposit, Hunan Province, South China. *Acta Petrol. Sin.* **2012**, *28*, 3809–3822. (In Chinese)
42. Ding, T.; Ma, D.S.; Lu, J.J.; Zhang, R.Q.; Zhang, S.T. S, Pb, and Sr isotope geochemistry and genesis of Pb–Zn mineralization in the Huangshaping polymetallic ore deposit of southern Hunan Province, China. *Ore Geol. Rev.* **2016**, *77*, 117–132. [CrossRef]
43. Wang, Q.; Mo, N.; Mao, Y.D. S-isotope geochemical study of Shizhuyuan deposit. *Land Resour. Her.* **2017**, *14*, 64–68. (In Chinese)
44. Chen, B.; Ma, X.H.; Wang, Z.Q. Origin of the fluorine-rich highly differentiated granites from the Qianlishan composite plutons (South China) and implications for polymetallic mineralization. *J. Asian Earth Sci.* **2014**, *93*, 301–314. [CrossRef]
45. Zheng, Y.F.; Xiao, W.J.; Zhao, G.C. Introduction to tectonics of China. *Gondwana Res.* **2013**, *23*, 1189–1206. [CrossRef]
46. Li, X.H.; Li, W.X.; Li, Z.X.; Lo, C.H.; Wang, J.; Ye, M.F.; Yang, Y.H. Amalgamation between the Yangtze and Cathaysia Blocks in South China: Constraints from SHRIMP U–Pb zircon ages, geochemistry and Nd–Hf isotopes of the Shuangxiwu volcanic rocks. *Precambrian Res.* **2009**, *174*, 117–128. [CrossRef]
47. Wang, X.L.; Shu, L.S.; Xing, G.F.; Zhou, J.C.; Tang, M.; Shu, X.J.; Qi, L.; Hu, Y.H. Post-orogenic extension in the eastern part of the Jiangnan orogen: Evidence from ca 800–760Ma volcanic rocks. *Precambrian Res.* **2012**, *222–223*, 404–423. [CrossRef]
48. Zhang, S.B.; Wu, R.X.; Zheng, Y.F. Neoproterozoic continental accretion in South China: Geochemical evidence from the Fuchuan ophiolite in the Jiangnan orogen. *Precambrian Res.* **2012**, *220–221*, 45–64. [CrossRef]
49. Zhang, S.B.; Zheng, Y.F. Formation and evolution of Precambrian continental lithosphere in South China. *Gondwana Res.* **2013**, *23*, 1241–1260. [CrossRef]
50. Zhao, G. Jiangnan Orogen in South China: Developing from divergent double subduction. *Gondwana Res.* **2015**, *27*, 1173–1180. [CrossRef]
51. Li, H.; Wu, Q.H.; Evans, N.J.; Zhou, Z.K.; Kong, H.; Xi, X.S.; Lin, Z.W. Geochemistry and geochronology of the Banxi Sb deposit: Implications for fluid origin and the evolution of Sb mineralization in central-western Hunan, South China. *Gondwana Res.* **2018**, *55*, 112–134. [CrossRef]
52. Zhou, X.M.; Sun, T.; Shen, W.Z.; Shu, L.S.; Niu, Y.L. Petrogenesis of Mesozoic granitoids and volcanic rocks in South China: A response to tectonic evolution. *Episodes* **2006**, *29*, 26–33.

53. Li, H.; Palinkaš, L.A.; Watanabe, K.; Xi, X.S. Petrogenesis of Jurassic A-type granites associated with Cu–Mo and W–Sn deposits in the central Nanling region, South China: Relation to mantle upwelling and intra-continental extension. *Ore Geol. Rev.* **2018**, *92*, 449–462. [CrossRef]
54. Xu, X.; O'Reilly, S.Y.; Griffin, W.L.; Deng, P.; Pearson, N.J. Relict Proterozoic basement in the Nanling Mountains (SE China) and its tectonothermal overprinting. *Tectonics* **2005**, *24*. [CrossRef]
55. Wang, Y.J.; Fan, W.M.; Sun, M.; Liang, X.Q.; Zhang, Y.H.; Peng, T.P. Geochronological, geochemical and geothermal constraints on petrogenesis of the Indosinian peraluminous granites in the South China Block: A case study in the Hunan Province. *Lithos* **2007**, *96*, 475–502. [CrossRef]
56. Li, J.H.; Dong, S.W.; Zhang, Y.Q.; Zhao, G.C.; Johnston, S.T.; Cui, J.J.; Xin, Y.J. New insights into Phanerozoic tectonics of south China: Part 1, polyphase deformation in the Jiuling and Lianyunshan domains of the central Jiangnan Orogen. *J. Geophys. Res. Solid Earth* **2016**, *121*, 3048–3080. [CrossRef]
57. Shu, L.S.; Zhou, X.M.; Deng, P.; Yu, X.Q.; Wang, B.; Zu, F.P. Geological features and tectonic evolution of Meso-Cenozoic basins in southeastern China. *Geol. Bull. China* **2004**, *23*, 876–884. (In Chinese)
58. Shu, L.S.; Wang, D.Z. A comparison study of basin and range tectonics in the Western North America and southeastern China. *Geol. J. China Univ.* **2006**, *12*, 1–13. (In Chinese)
59. Shu, L.S.; Zhou, X.M.; Deng, P.; Wang, B.; Jiang, S.Y.; Yu, J.H.; Zhao, X.X. Mesozoic tectonic evolution of the Southeast China Block: New insights from basin analysis. *J. Asian Earth Sci.* **2009**, *34*, 376–391. [CrossRef]
60. Yao, J.M.; Hua, R.M.; Lin, J.F. Zircon LA-ICP-MS U-Pb dating and geochemical characteristics of Huangshaping granite in southeast Hunan Province, China. *Acta Petrol. Sin.* **2005**, *21*, 688–696. (In Chinese)
61. Li, H.; Watanabe, K.; Yonezu, K. Zircon morphology, geochronology and trace element geochemistry of the granites from the Huangshaping polymetallic deposit, South China: Implications for the magmatic evolution and mineralization processes. *Ore Geol. Rev.* **2014**, *60*, 14–35. [CrossRef]
62. Ding, T.; Ma, D.S.; Lu, J.J.; Zhang, R.Q.; Zhang, S.T.; Gao, S.Y. Petrogenesis of Late Jurassic granitoids and relationship to polymetallic deposits in southern China: The Huangshaping example. *Int. Geol. Rev.* **2016**, *58*, 1646–1672. [CrossRef]
63. Ding, T.; Ma, D.S.; Lu, J.J.; Zhang, R.Q.; Zhang, S.T. Mineral geochemistry of granite porphyry in Huangshaping pollymetallic deposit, southern Hunan Province, and its implications for metallogensis of skarn scheelite mineralization. *Acta Petrol. Sin.* **2017**, *33*, 716–728. (In Chinese)
64. *Verification Report on the Reserves of the Shizhuyuan Deposit*; Southern Hunan Geological Survey Institute: Chenzhou, China, Unpublished work; 2015. (In Chinese)
65. Mao, J.W.; Li, H.Y.; Guy, B.; Raimbault, L. Geology and metallogeny of the Shizhuyuan skarn-greisen W–Sn–Mo–Bi deposit, Hunan Province. *Miner. Depos.* **1996**, *15*, 1–15. (In Chinese)
66. Jiang, Y.H.; Jiang, S.Y.; Zhao, K.D.; Ling, H.F. Petrogenesis of Late Jurassic Qianlishan granites and mafic dykes, Southeast China: Implications for a back-arc extension setting. *Geol. Mag.* **2006**, *143*, 457–474. [CrossRef]
67. Guo, C.L.; Wang, R.C.; Yuan, S.D.; Wu, S.H.; Yin, B. Geochronological and geochemical constraints on the petrogenesis and geodynamic setting of the Qianlishan granitic pluton, Southeast China. *Miner. Petrol.* **2014**, *109*, 253–282. [CrossRef]
68. Chen, Y.X.; Li, H.; Sun, W.D.; Ireland, T.; Tian, X.F.; Hu, Y.B.; Yang, W.B.; Chen, C.; Xu, D.R. Generation of Late Mesozoic Qianlishan A2-type granite in Nanling Range, South China: Implications for Shizhuyuan W–Sn mineralization and tectonic evolution. *Lithos* **2016**, *266–267*, 435–452. [CrossRef]
69. Li, X.H.; Liu, D.Y.; Sun, M.; Li, W.X.; Liang, X.R.; Liu, Y. Precise Sm–Nd and U–Pb isotopic dating of the supergiant Shizhuyuan polymetallic deposit and its host granite, SE China. *Geol. Mag.* **2004**, *141*, 225–231. [CrossRef]
70. Mao, J.W. Metallogenic speciality of super giant polymetallic tungsten deposit: Taking the Shizhuyuan deposit as an example. *Sci. Geol. Sin.* **1997**, *32*, 351–363. (In Chinese)
71. Zhu, X.Y.; Wang, J.B.; Wang, Y.L.; Chen, X.Y. The role of magma-hydrothermal transition fluid in the skarn-type tungsten mineralization process: A case study from the Shizhuyuan tungsten and tin polymetallic ore deposit. *Acta Petrol. Sin.* **2015**, *31*, 891–905. (In Chinese)
72. Xiong, X.L.; Rao, B.; Chen, F.R.; Zhu, J.C.; Zhao, Z.H. Crystallization and melting experiments of a fluorine-rich leucogranite from the Xianghualing Pluton, South China, at 150 MPa and H_2O-saturated conditions. *J. Asian Earth Sci.* **2002**, *21*, 175–188. [CrossRef]

73. Zhu, J.C.; Wang, R.C.; Lu, J.J.; Zhang, H.; Zhang, W.L.; Xie, L.; Zhang, R.Q. Fractionation, evolution, petrogenesis and mineralization of Laiziling granite pluton, southern Hunan Province. *Geol. J. China Univ.* **2011**, *17*, 381–392. (In Chinese)
74. Yang, L.Z.; Wu, X.B.; Cao, J.Y.; Hu, B.; Zhang, X.W.; Gong, Y.S.; Liu, W.D. Geochronology, Petrology, and Genesis of Two Granitic Plutons of the Xianghualing Ore Field in South Hunan Province: Constraints from Zircon U–Pb Dating, Geochemistry, and Lu–Hf Isotopic Compositions. *Minerals* **2018**, *8*, 213. [CrossRef]
75. Yin, J.W.; Lee, H.K.; Chio, K.K.; Kim, S.J. Characteristics of garnet in Shizhuyuan skarn deposit, Hunan province. *Earth Sci.-J. China Univ. Geosci.* **2000**, *25*, 163–171. (In Chinese)
76. Li, H.; Wu, J.H.; Evans, J.E.; Jiang, W.C.; Zhou, Z.K. Zircon geochronology and geochemistry of the Xianghualing A-typegranitic rocks: Insights into multi-stage Sn-polymetallic mineralization in South China. *Lithos* **2018**, *312–313*, 1–20. [CrossRef]
77. Cheng, Y.S.; Huang, H.M. Geochemical characteristics and mineralization indication of Devonian strata in Dachang ore field, Guangxi. *Chin. J. Nonferr. Met.* **2012**, *23*, 2649–2658. (In Chinese)
78. Sun, S.S.; McDonough, W.F. Chemical and isotopic systematics of oceanic basalts: Implications for mantle compositions and processes. In *Magmatism in the Ocean Basins*; Saunders, A.D., Norry, M.J., Eds.; Geological Society, London Special Publication: London, UK, 1989; Volume 32, pp. 313–345.
79. Li, H.; Myint, A.Z.; Yonezu, K.; Watanabe, K.; Algeo, T.J.; Wu, J.H. Geochemistry and U–Pb geochronology of the Wagone and Hermyingyi A-type granites, southern Myanmar: Implications for tectonic setting, magma evolution and Sn–W mineralization. *Ore Geol. Rev.* **2018**, *95*, 575–592. [CrossRef]
80. Halliday, A.N.; Davidson, J.P.; Hildreth, W.; Holden, P. Modelling the petrogenesis of high Rb/Sr silicic magmas. *Chem. Geol.* **1991**, *92*, 107–114. [CrossRef]
81. Li, F.L.; Chen, D.X.; Zhang, B.R. Geochemical characteristics and metallization of the strata in South Hunan. *Earth Sci.-J. China Univ. Geosci.* **1996**, *21*, 535–540. (In Chinese)
82. Ai, H. Zircon U–Pb geochronology and Hf isotopic compositions of ore-related granites from Huangshaping polymetallic deposit of Hunan Province. *Miner. Depos.* **2013**, *32*, 545–563. (In Chinese)
83. Wang, H. *Huangshaping Lead-Zinc Deposit Ore-Forming Fluid Geochemistry and Depth Estimation*; China University of Geoscience: Beijing, China, 2013. (In Chinese)
84. Meinert, L.D. Application of skarn deposit zonation models to mineral exploration. *Explor. Min. Geol.* **1997**, *6*, 185–208.
85. Ishihara, S.; Lee, D.S.; Kim, S.Y. Comparative study of Mesozoic granitoids and related W-Mo mineralization in Southern Korea and Southwestern Japan. *Min. Geol.* **1981**, *31*, 311–320.
86. Liu, Y.M.; Lu, H.Z.; Wang, C.L.; Xu, Y.Z.; Kang, W.Q.; Zeng, T. On the ore-forming conditions and ore-forming model of the superlarge multimetal deposit in Shizhuyuan. *Sci. China Ser. D* **1998**, *41*, 502–512. [CrossRef]